Science Advances
AAAS

Supplementary Materials for

Low case numbers enable long-term stable pandemic control without lockdowns

Sebastian Contreras, Jonas Dehning, Sebastian B. Mohr, Simon Bauer, F. Paul Spitzner, Viola Priesemann*

*Corresponding author. Email: viola.priesemann@ds.mpg.de

Published 8 October 2021, *Sci. Adv.* **7**, eabg2243 (2021)
DOI: 10.1126/sciadv.abg2243

This PDF file includes:

S1 Supplementary Notes of "Low case numbers enable long-term stable pandemic control without lockdowns"

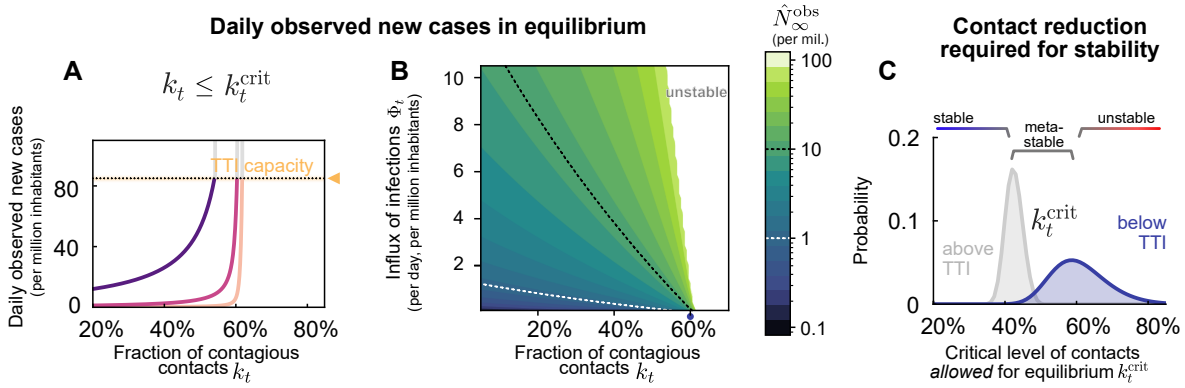

Supplementary Figure S1: **In the stable and metastable regimes, daily new cases approach an equilibrium value $\hat{N}_\infty^{\text{obs}}$ that depends on the level of contacts k_t and an external influx of new cases Φ_t. A:** The equilibrium value $\hat{N}_\infty^{\text{obs}}$ increases steeply with higher k_t and then destabilizes when surpassing a critical value k_t^{crit}. Thus, contact reduction has to be sufficiently strong to keep the case numbers within TTI capacity. A certain degree of external influx Φ_t can be compensated, but in general, Φ_t can put stability at risk. $\Phi_t = 1$ one daily new case per million is our default parameter for the influx. **B:** The $\hat{N}_\infty^{\text{obs}}$ is below 10 for a large fraction of combinations of k_t and Φ_t, thus well below the capacity limit of TTI. **C:** The critical value k_t^{crit}, which marks the transition between stable and (meta)stable spread; thus k_t^{crit} displays the maximal level of contacts that is allowed while controlling the spread (and stabilize case numbers). If case numbers are below the TTI capacity limit, a contact level of at most $k_t^{\text{crit}} = 61\,\%$ is allowed for stabilization (blue). If case numbers, however, are above the TTI limit, stronger contact reduction is necessary for stabilization, thus allowing a lower level of contacts ($k_t^{\text{crit}} = 42\,\%$, gray). Confidence intervals originate from error propagation of the uncertainty of the underlying model parameters. All model parameters are listed in Supplementary Table S1 and the full uncertainty analysis is in Fig. S2.

S1.1 Strategies to face COVID-19 differ among countries.

Several South- and East-Asian countries and Australia, and New Zealand have achieved very low case numbers and even local eradication. These countries reached very low values below one daily new case per million (median 0.5, Fig. 6 C). If local eradication is successful, these countries can profit from the absorbing state of zero SARS-CoV-2 infections, i.e. after local eradication, new infection chains are only started if a virus is *de novo* carried into the country (*67, 68*). However, the local eradication is constantly put at risk by the undetected influx of new viruses from abroad, requiring rigorous quarantine for international travel, and – once the spread got out of control – decisive action to completely stop all infection chains. However, the more countries adhere to this strategy successfully, the closer one may get to global eradication.

In many European countries over the summer, case numbers were relatively low, typically around ten daily new cases per million (Fig. 6 B). During that time, contacts were only mildly or moderately restricted, and containment was complemented by hygiene, masks, and other preventive measures. However, in summer and autumn, most European countries developed a second wave Fig. S5. The causes are undoubtedly diverse, from increasing contact rates to seasonal effects and travel-related influx. Seasonal effects alone cannot explain the second wave, as neighboring countries like Portugal versus Spain or Finland versus Sweden show remarkably different dynamics (see (*35*)). Hence, it seems to be possible to maintain an equilibrium at relatively low case numbers. However, that equilibrium is fragile at high case numbers, and novel waves can emerge at any time.

Sustained high levels of case numbers have been observed in several countries such that TTI probably could not be performed effectively. Around 130 daily new cases per million have been observed, e.g. in many (but not all) American countries (median 129.54, Fig. 6 A). It shows that high levels of daily new infections

can be maintained in principle. However the stringency of interventions is similar or higher compared to other countries (see (*36*)), and even with these high numbers it will probably take about $200\,000/150 = 1333$ to $700\,000/150 = 4666$ days, thus several years, until 20 to 70 % of the population is infected and population immunity reached – assuming the duration of individual immunity is long enough. That high level of new infections leads to a considerable death toll, as currently about 1.5 % of the infected individuals would die (depending on age structure (*2, 16*)). Moreover, containment measures like quarantine become unsustainable because, if implemented, each one of the 200 daily new infected cases would require the quarantine of 5-50 people (their high-risk contacts) for about ten days, causing 1 - 10 % of the population being in quarantine at any given day. Therefore the alleged economic and social benefits of such a strategy (*3, 7*) may be questionable.

S1.2 Linear stability analysis and uncertainty propagation

For analyzing the stability of the governing differential equations, namely, whether an outbreak could be controlled, we studied the linear stability of the system. Moreover, we consider that, within the time-frame considered for stability purposes, the fraction $\frac{S}{M}$ would remain somewhat constant, we consider the linearized version of equations (3)– (7), defining a system of delay differential equations for the variables $x(t) = \left[E^Q(t);\, E^H(t);\, I^Q(t);\, I^H(t);\, I^{H,s}(t)\right]$. We define matrices A and B as:

$$A = \begin{pmatrix} -\rho & 0 & \nu\gamma R_0 & 0 & 0 \\ 0 & -\rho & \epsilon\gamma R_0 & \gamma k_t R_0 & 0 \\ \rho & 0 & -\gamma & \lambda_r & \lambda_s \\ 0 & \rho & 0 & -\gamma-\lambda_r & -\lambda_s \\ 0 & (1-\xi)\,\rho & 0 & 0 & -\gamma-\lambda_r-\lambda_s \end{pmatrix} \tag{1}$$

$$B = \begin{pmatrix} 0 & 0 & 0 & \lambda_r^{\text{eff}}\chi_\tau & \lambda_s^{\text{eff}}\chi_\tau \\ 0 & 0 & 0 & -\lambda_r^{\text{eff}}\chi_\tau & -\lambda_s^{\text{eff}}\chi_\tau \\ 0 & 0 & 0 & \lambda_r^{\text{eff}}\left(\xi\chi_r + (1-\xi)\,\chi_{s,r}\right) & \lambda_s^{\text{eff}}\left(\xi\chi_r + (1-\xi)\,\chi_{s,r}\right) \\ 0 & 0 & 0 & -\lambda_r^{\text{eff}}\left(\xi\chi_r + (1-\xi)\,\chi_{s,r}\right) & -\lambda_s^{\text{eff}}\left(\xi\chi_r + (1-\xi)\,\chi_{s,r}\right) \\ 0 & 0 & 0 & -\lambda_r^{\text{eff}}\,(1-\xi)\,\chi_{s,r} & -\lambda_s^{\text{eff}}\,(1-\xi)\,\chi_{s,r} \end{pmatrix} \eta k_t R_0, \tag{2}$$

where

$$\lambda_r^{\text{eff}} = \frac{\gamma\lambda_r}{\lambda_r+\gamma}, \qquad \lambda_s^{\text{eff}} = \gamma\left(\frac{\lambda_s+\lambda_r}{\gamma+\lambda_s+\lambda_r} - \frac{\lambda_r}{\lambda_r+\gamma}\right). \tag{3}$$

The equations governing the dynamics for vector $x(t)$ are then presented in their matrix form:

$$x'(t) = Ax(t) + Bx(t-\tau). \tag{4}$$

We determine the maximum –critical– level of contacts k_t^{crit}, for which exponential solutions would be asymptotically stable. Eigenvalues were determined by systematically solving the nonlinear eigenvalues problem for stability (*61*), where the solution operation was approximated with a Chebyshev differentiation matrix (*62*). Eigenvalues, in this sense, would be solutions of the scalar equation

$$\det\left(-sI + A + e^{-s\tau}B\right) = 0 \tag{5}$$

Noting that A and B explicitly depend on the model parameters, we numerically explore which combinations would result in stable, metastable, or unstable case numbers. Concretely, we studied the maximum –critical– level of contacts allowed for stability k_t^{crit} in two scenarios; i) low case numbers, and TTI fully operative (both testing and contact tracing), and ii) high case numbers, above the TTI limit, where testing would be inefficient and solely symptom driven ($\lambda_s = \lambda_s'$, $\eta = \lambda_r = \lambda_r' = 0$).

To explore the uni-variate impact different signature parameters have on k_t^{crit}, we studied the zeros of (5) as a function of k_t using the `@fzero` MATLAB function (Fig. S2A). Using the same routines and a random sampling procedure, we propagate uncertainties in the values of these parameters, uni-variate (Fig. S2B), and multivariate (Fig. S2C).

Supplementary Table S1: Parameter uncertainty propagation. α and β are the shape parameters of the beta distribution.

Parameter	Meaning	Median	95% CI	α	β	Dist.	Units
ξ	Asymptomatic ratio	0.32	0.23–0.42	27.5	27.8	beta	–
λ_s	Symptom-driven test rate	0.25	0.20–0.31	56	168	beta	days^{-1}
ν	Registered contacts (quarantined)	0.07	0.03–0.13	8.25	101.8	beta	–
η	Tracing efficiency	0.66	0.59–0.73	117.9	60.7	beta	–
ϵ	Lost contacts (quarantined)	0.05	0.01–0.11	3.8	71.25	beta	–
$k_t^{\text{crit}}\big\vert_{\text{TTI}}$	Maximum –critical– level of contacts allowed for stability (with TTI)	61 %	47–76 %	–	–	–	–
$k_t^{\text{crit}}\big\vert_{\text{no TTI}}$	Maximum –critical– level of contacts allowed for stability (without TTI)	42 %	38–47 %	–	–	–	–

Supplementary Table S2: Linearly-derived correspondence between contact reduction and the observed reproduction number

k_t	$\hat{R}_t^{\text{obs}}$ (with TTI)	$\hat{R}_t^{\text{obs}}$ (without TTI)
0.8	1.08	1.26
0.6	0.99	1.13
0.4	0.91	0.98
0.25	0.86	0.88

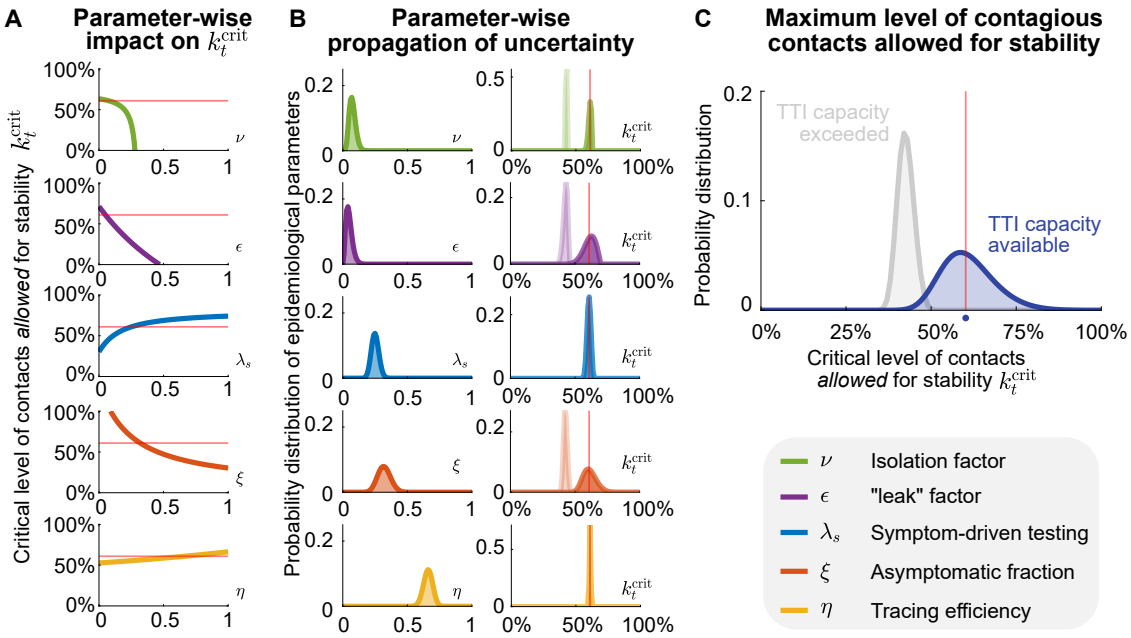

Supplementary Figure S2: **Propagation of TTI-parameter uncertainties to the critical level of contacts allowed for stability.** As the different parameters involved in our model play different roles, the way their variability propagates to k_t^{crit} differs, even when their variability profiles look similar. **A:** Impact of single-parameter variation on the critical (maximal, allowed) level of contagious contacts k_t^{crit}. To evaluate the monotony (direction) of their impact on k_t^{crit}, we scan their entire definition range, ignoring the practical feasibility of achieving such values. The solid red line shows the default critical level of contacts allowed for stability. **B:** Univariate uncertainties of TTI parameters modeled by beta distributions centered on their default value, and the resulting distribution of critical fraction of contagious contacts k_t^{crit} (right column). Results are shown assuming testing only (light colors) or testing and tracing (dark colors). Solid red lines represent the default value of k_t^{crit} in the regime of available TTI capacity. **C:** Distribution of the critical fraction of contacts arising from multivariate uncertainty propagation given by the joint of the distributions shown in (A) for testing only (light colors) or testing and tracing (dark colors). Solid red lines represent the default value of k_t^{crit} in the regime of available TTI capacity. Results show averages of 100 000 realizations.

S1.3 On the contact reduction required for achieving early population immunity.

In Supplementary Section S1.2, we derived a methodology for obtaining the minimal, critical contact reduction k_t^{crit} for which the linear system is asymptotically stable. Such values, however, assume a fully susceptible population, as we ignore the scaling factor $\frac{S}{M}$.

The population immunity threshold ϱ represents the fraction of the population that needs to be immunized for controlling the spread of an infectious disease. It can be expressed in terms of the effective reproduction number R_t:

$$\varrho = 1 - \frac{1}{R_t}. \tag{6}$$

In the context of our model, R_t can be expressed in terms of the fraction of contagious contacts k_t and the basic reproduction number R_0; $R_t = k_t R_0$. However, in further stages of an ongoing outbreak, the fraction of people no longer susceptible would affect the spread. Thus we include also the scaling factor $\frac{S}{M}$:

$$R_t = k_t \frac{S}{M} R_0. \tag{7}$$

Combining both equation (6) and (7), we can express ϱ as

$$\varrho = 1 - \frac{1}{k_t\,(1-f)\,R_0}, \tag{8}$$

assuming a quasi-stationary dynamics for S, and defining $f = 1 - \frac{S}{M}$. Suppose we study the case in which no major behavioral changes take place. Thus the population immunity threshold ϱ would remain the same. On the other hand, because of the sole fact of having a progressively increasing immunization among the population (because of vaccination or post-infection immunity), the maximal allowed level of contacts k_t^{crit} will increase. Assuming critical conditions, we use $k_t = k_t^{\text{crit}}$ in equation (8):

$$\varrho = 1 - \frac{1}{k_t^{\text{crit}}\,(1-f)\,R_0}, \tag{9}$$

As we assumed that no behavioral change is taking place, we obtain the population immunity threshold by only evaluating equation (9) at $f = 0$.

$$\varrho = 1 - \frac{1}{k^{\text{crit},0} R_0}, \tag{10}$$

where $k^{\text{crit},0}$ represents the critical level of contacts allowed in a fully susceptible population, and can be calculated directly from the linear stability analysis described in S1.2. Subtracting (9) and (10) we obtain an expression for $k_t^{\text{crit}}(f)$

$$k_t^{\text{crit}}(f) = \frac{k^{\text{crit},0}}{1-f}. \tag{11}$$

Finally, this expression only depends on the remaining susceptible population $(1-f)$, and on the critical level of contacts when $f = 0$. Note that this equation can return values of $k_t^{\text{crit}}(f)$ larger than one, should f be *close enough* to one. Following our interpretation of $k_t^{\text{crit}}(f)$, that would mean reaching the population immunity level, as individuals would be allowed to have even higher levels of contacts than those they had before COVID-19.

S1.4 Calculating the increase in the level of contacts allowed with increased immunity

In the previous section, we demonstrated that with increased immunity (acquired by vaccination or post-infection), the maximum –critical– level of contacts k_t^{crit} allowed for stability would increase. We also discussed that, as a first-order approach, the level at which the system is stabilized (namely, $\hat{N}_\infty^{\text{obs}}$) is determined by the influx Φ_t and the distance between the current level of contacts k_t and k_t^{crit} according to the formula

$$\hat{N}_\infty^{\text{obs}} = \frac{\Phi_t}{k_t^{\text{crit}} - k_t}. \tag{12}$$

We can re-write equation (12) as:

$$k_t = \frac{k^{\text{crit},0}}{1-f} - \frac{\Phi_t}{\hat{N}_\infty^{\text{obs}}}, \tag{13}$$

where k_t represents the *allowed* level of contagious contacts so that the distance to the singularity (reached if $k_t = k_t^{\text{crit}}$) is kept constant. According to equation (13), increasing levels of immunity will lead to higher critical level of contacts, thus allowing individuals to steadily increase the level of contagious contacts k_t while still keeping the same equilibrium value for case numbers.

In order to connect this quantity to the predominant circulating variants, we recall the definition of the hidden reproduction number R_t^H (which is slightly different from the effective reproduction number R_t

defined in equation (7)). As described in the main text and in (*15*), R_t^H accounts for the number of offspring infections generated by individuals unaware of being infectious, in a fully susceptible population. In that way, we can express it in terms of k_t; $R_t^H = k_t R_0$. Thus, we can rewrite equation (13) in terms of the allowed hidden reproduction number R_t^H, just by multiplying it by R_0.

$$R_t^H = \frac{k_t^{\mathrm{crit},0} R_0}{1-f} - \frac{\Phi_t R_0}{\hat{N}_\infty^{\mathrm{obs}}}, \tag{14}$$

We note a slight coupling between the hidden reproduction number R_t^H and the dominant variant of SARS-CoV-2 (through the base reproduction number), so scenarios need to be analyzed separately. Using the vaccination progress described in Fig. 5 in the main text, our results are summarized in Fig. S3, where we assume that the TTI and hospital strategies (resp. blue and gray curves) stabilize at 10 and 250 cases per million people, respectively. The influx term that reduces the allowed hidden reproduction number R_t^H highlights the need of combining NPIs aiming to lower case numbers to the TTI regime (where $k_t^{\mathrm{crit},0}$ is higher), especially when large fractions of the population remain susceptible (cf. Fig. S3A). However, in the presence of highly contagious variants, NPIs must remain in place, as even after vaccine rollout the allowed hidden reproduction number could not surpass the base reproduction number of the variant. Even though reducing the influx could also help, its effect is little compared with the effect of immunization (cf. Fig. S3B).

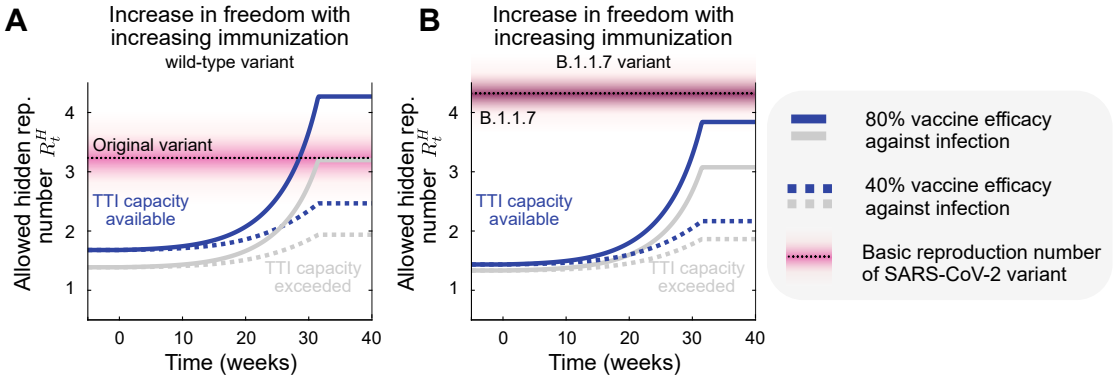

Supplementary Figure S3: **As growing immunity increases the maximal allowed number of contacts, freedom will proportionally increase.** Scenarios considering the original, wild-type variant of SARS-CoV-2 ($R_0 = 3.3$) show that vaccination together with a strategy aiming at low case numbers can make the allowed hidden reproduction number R_t^H cross the variant's R_0, i.e., the population immunity threshold (**A**). However, considering the higher reproduction number of the B.1.1.7, restrictions are not allowed to be lifted fully to keep case numbers under control, even if within TTI capacity (**B**). The vaccination progress here was adapted from Figure 5 from the main text.

S1.5 Inferring the reproduction number of COVID-19 from Jun to Oct. 2020

We use the Bayesian inference framework on an SIR model presented in our previous work (*17*) to infer the daily growth rate $\lambda^*(t)$. An SIR compartmental model with weekly change points is used whose main epidemiological parameters are inferred using the PyMC3 package (*69*). A weekly modulation was applied to take the weekly reporting structure and weekend delays into account. After inference, a rolling average was performed on the daily case numbers for comparability and clarity. The observed reproduction number $\hat{R}_t^{\mathrm{obs}}$ can be expressed depending on the effective daily growth rate:

$$\hat{R}_t^{\mathrm{obs}} = (\lambda^*(t) + 1)^4 \tag{15}$$

This short analysis was performed for Germany (Fig. S4) and other European countries (Fig. S5), which showed the same metastable behavior, while their case numbers were below a threshold of around 50 cases

per day (per million). A transition into the unstable regime can be seen once case numbers surpass this threshold.

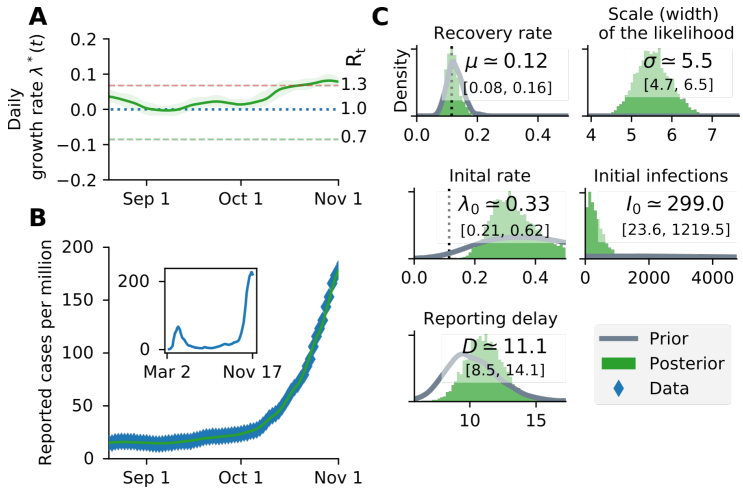

Supplementary Figure S4: **A substantial increase in Germany's effective growth rate occurred during October, suggesting that regional TTI capacity limits were exceeded.** (**A**) Before October, the reproduction number was slightly above one (corresponding to a daily growth rate λ^* slightly above zero). (**B**) Observed case numbers were stabilized below 20 daily new cases per million (but still slowly growing) until a transition into the unstable regime took place over ~ 4 weeks in October. The time range is adjusted to focus on this tipping point. The inset shows case numbers for the full available time range. (**C**) Main central epidemiological parameters with the prior and posterior distribution.

S1.6 On the incorporation of random testing in the TTI scheme

Testing can also be done randomly or randomly combined with a contact tracing strategy. Even though the number of tests required for such purposes would be enormous, the development of fast, cheap, and reliable tests offers an exciting alternative to consider.

In this supplementary note, we derive the equations presented in the methods but also including random testing. As therein described, random testing is assumed to occur at a constant rate λ_r, which, for default parameters, reflect the number of tests per day per million people. In that way, it seems reasonable to consider unfeasible testing rates surpassing $\lambda_r^{\max} = 0.1$, as it would mean that a 10 % of the population is tested every day.

S1.6.1 Number of cases observable through testing N^{test}

When random testing is included in the scheme, the solution of equation (19) for the symptomatic and asymptomatic infections -hidden- would be given by equations (16) and (17).

$$\chi_{s,r} = \begin{cases} \rho\tau \exp\left(-\rho\tau\right), & \text{if } \rho \approx \lambda_s + \lambda_r \\ \dfrac{\rho}{(\lambda_s + \lambda_r) - \rho} \left(\exp\left(-\rho\tau\right) - \exp\left(-\tau\left(\lambda_s + \lambda_r\right)\right)\right), & \text{else.} \end{cases} \tag{16}$$

$$\chi_{r} = \begin{cases} \rho\tau \exp\left(-\rho\tau\right), & \text{if } \rho \approx \lambda_r \\ \dfrac{\rho}{\lambda_r - \rho} \left(\exp\left(-\rho\tau\right) - \exp\left(-\tau\lambda_r\right)\right), & \text{else.} \end{cases} \tag{17}$$

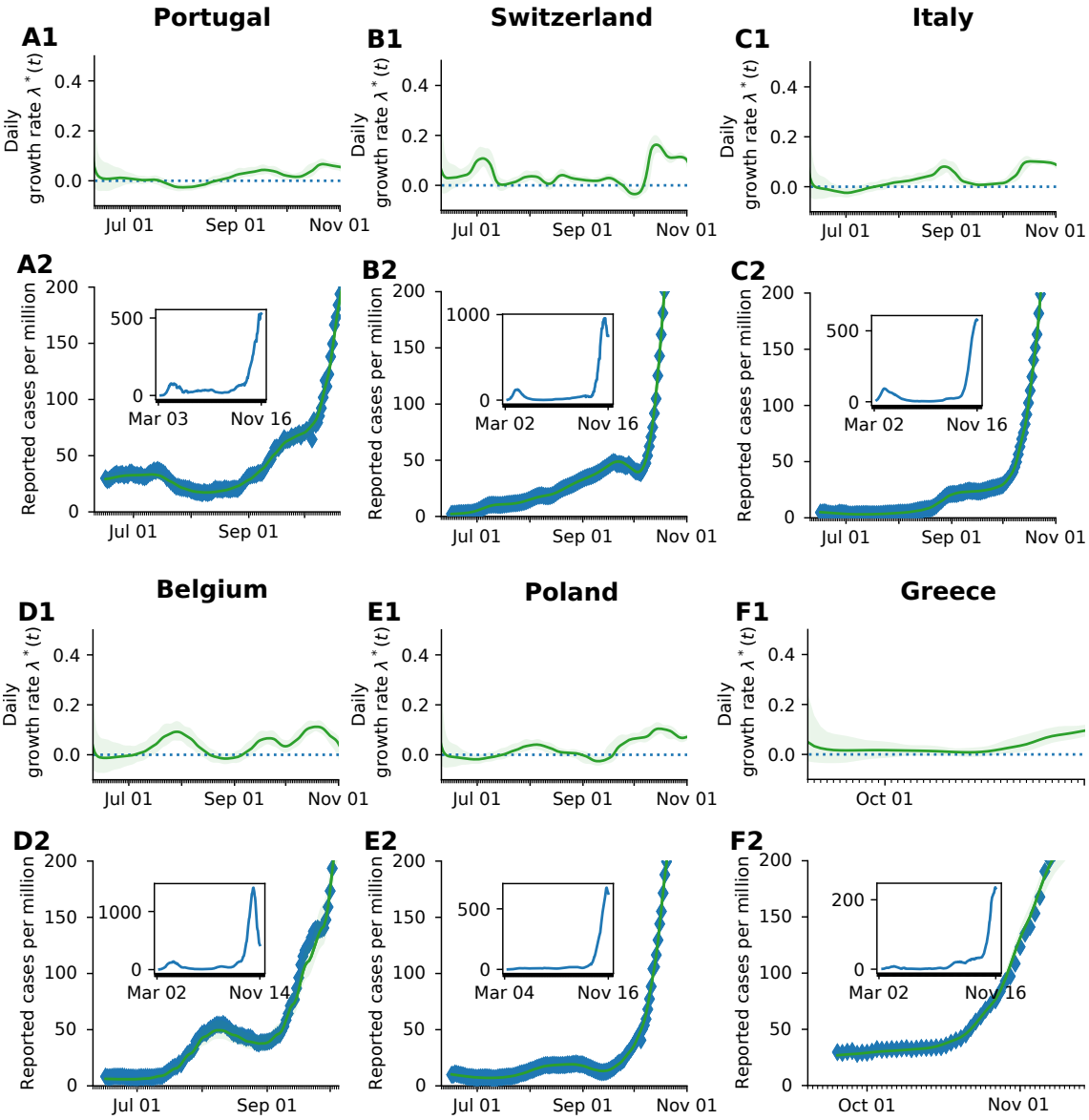

Supplementary Figure S5: **Comparison of the reproduction number and reported cases as the second wave emerges in different European countries.** For each country, parameters of an SIR model, were fitted to the reported data of the Our World in Data repository (*35*), following the procedure presented in (*17*). (**Panels X1**) The time-dependent effective growth rate stays between -0.1 and 0.1 and rises before the tipping point. This corresponds to an effective reproduction number between 0.7 and 1.3, which matches our preliminary assumptions. The time range is adjusted to focus on the tipping point. (**Panels X2**) After a (meta-)stable regime in summer, all selected countries show a rise in case numbers and a tipping point at around 50 new cases per day per million. The spread self-accelerates, and the cases increase significantly. (**Insets**) Case numbers for the full available time range.

If both symptom-based and random testing take place simultaneously, the number of discovered infections is given by

$$N^{\text{test}} = \lambda_r I^H + \lambda_s I^{H,s} \tag{18}$$

Further, assuming that after reaching $N^{\text{test}}_{\text{max}}$, the testing rates at the overhead pool-sizes would decrease to λ'_s and λ'_r, respectively, for symptom-driven and random testing. We further assume that testing resources

would be exclusively allocated to sustain the symptom-driven testing in our default scenario. The overall testing term N^{test} would be given by:

$$\begin{aligned} N^{\text{test}} = \lambda_r \min\left(I^H, I^H_{\max}\right) + \lambda'_r \max\left(0, I^H - I^H_{\max}\right) \\ + \lambda_s \min\left(I^{H,s}, I^{H,s}_{\max}\right) + \lambda'_s \max\left(0, I^{H,s} - I^{H,s}_{\max}\right), \end{aligned} \tag{19}$$

where $I^{H,s}_{\max}, I^H_{\max}$ represent the pool sizes of the symptomatic hidden and total hidden pools, respectively, at the TTI limit, i.e. $\lambda_r I^H_{\max} + \lambda_s I^{H,s}_{\max} \stackrel{!}{=} N^{\text{test}}_{\max}$, reached at time $t = t^*$. Defining $\varphi := \left.\frac{I^{H,s}}{I^H}\right|_{t=t^*}$, we can express such magnitudes in term of the maximum capacity $N^{\text{test}}_{\max}$:

$$I^{H,s}_{\max} = \frac{\varphi N^{\text{test}}_{\max}}{\varphi\lambda_s + \lambda_r} \tag{20}$$

$$I^H_{\max} = \frac{N^{\text{test}}_{\max}}{\varphi\lambda_s + \lambda_r}. \tag{21}$$

The explicit value of φ can be obtained numerically in the integration routine or estimated through the use of the equilibrium values of the differential equations, $\varphi = \frac{I^{H,s}_\infty}{I^H_\infty}$ (as implemented in our code). The expression for the symptomatic hidden pool $I^{H,s}$ in the presence of random testing is slightly different;

$$\begin{aligned} N^{\text{test}}_s = \lambda_r \min\left(I^{H,s}, I^{H,s}_{\max}\right) + \lambda'_r \max\left(0, I^{H,s} - I^{H,s}_{\max}\right) \\ + \lambda_s \min\left(I^{H,s}, I^{H,s}_{\max}\right) + \lambda'_s \max\left(0, I^{H,s} - I^{H,s}_{\max}\right). \end{aligned} \tag{22}$$

S1.6.2 Random testing: number of cases observable through contact-tracing N^{traced}

Because of TTI, infectious individuals move (or are likely to move) from the hidden to the quarantined infectious pool before recovering. Therefore, they spend a comparatively shorter amount of time there and, on average, would not generate the expected amount of offspring infections as some would be prevented. In the absence of TTI, the average time individuals spend in the infectious compartment is $\frac{1}{\gamma}$. In the presence of selective TTI, symptomatic individuals would have a greater chance to be tested (and thereby removed) than the asymptomatic ones. As we explicitly consider compartments for symptomatic and asymptomatic infections, each pool's residence times would be different. Noting that symptomatic individuals can be tested and therefore removed by any of the testing criteria, their residence time would be approximate $\frac{1}{\gamma+\lambda_s+\lambda_r}$. In contrast, the average residence time of asymptomatic individuals would be $\frac{1}{\gamma+\lambda_r}$. Therefore, the fractions of time that symptomatic and asymptomatic individuals stay unnoticed are respectively

$$t_s = \frac{\gamma}{\gamma + \lambda_s + \lambda_r}, \tag{23}$$

and

$$t_r = \frac{\gamma}{\gamma + \lambda_r}. \tag{24}$$

If the daily new cases observed through testing, delayed at the moment of processing, $N^{\text{test}}_{t-\tau}$, are within the tracing capacity of the health authorities, i.e. $N^{\text{test}}_{t-\tau} \leq N^{\text{test}}_{\max}$, then N^{traced} is defined as

$$N^{\text{traced}} = \eta R_{t-\tau}\left(I^H_{t-\tau} t_r \lambda_r + I^{H,s}_{t-\tau}\left(t_s\lambda_s + (t_s - t_r)\,\lambda_r\right)\right), \tag{25}$$

where $R_{t-\tau}$ represents the effective reproduction number, as defined in equation (7). Otherwise, using the expressions for I^H and $I^{H,s}$ when the TTI capacity is reached derived in the previous section, we can obtain an effective rate

$$\lambda_{\text{eq}} = \frac{\lambda_r \left((1-\varphi)\, t_r + \varphi t_s \right) + \varphi \lambda_s t_s}{\lambda_r + \varphi \lambda_s}. \tag{26}$$

Therefore, the average amount of positive cases identified by contact tracing in the TTI limit is given by

$$N^{\text{traced}} = \eta R_{t-\tau} N^{\text{test}}_{\max} \lambda_{\text{eq}}. \tag{27}$$

To sum up the last equations:

$$N^{\text{traced}} = \begin{cases} \eta R_{t-\tau} (I^H_{t-\tau} t_r \lambda_r + I^{H,s}_{t-\tau} \left(t_s \lambda_s + (t_s - t_r)\, \lambda_r \right)) & \text{if } N^{\text{test}}_{t-\tau} \leq N^{\text{test}}_{\max} \\ \eta R_{t-\tau} N^{\text{test}}_{\max} \lambda_{\text{eq}} & \text{else} \end{cases} \tag{28}$$

S1.7 More analytical insights into the TTI-based metastable regime

One of the crucial aspects of this paper is the description and profit from a metastable regime at low case numbers. Because of the different compartments at interplay in the dynamics, some metastability aspects are easier to present using a simplified model. The critical element behind the case-number dependent metastability is the limited capacity to perform contact tracing of the newly identified infections. We refer to the TTI limit being reached at a prevalence given by $I = I^{\max}$. However, the fact that this metastable equilibrium shows non-zero case numbers arises from a small but non-vanishing influx of externally acquired infections to the system, which we call Φ_t.

Aiming to illustrate the dynamics in a minimalist way, we proceed as follows. We modify a plain SIR model to include hidden and quarantined infections but simplify the TTI scheme to only depend on two parameters: the TTI capacity referred to the hidden incidence $I^{\max}_H$ and the testing rate λ as long as the capacity is not exceeded. If the capacity is exceeded the testing rate drops to zero. Infections in the quarantined and hidden pools spread at rates β_1 and β_2 respectively, with $\beta_1 < \beta_2$, and the recovery rate is given by γ:

$$\frac{dS}{dt} = -\beta_1 I^Q \frac{S}{M} - \beta_2 I^H \frac{S}{M} - \Phi_t \tag{29}$$

$$\frac{dI^Q}{dt} = \beta_1 I^Q \frac{S}{M} - \gamma I^Q + \min(\lambda I^H, \lambda I^H_{\max}) \tag{30}$$

$$\frac{dI^H}{dt} = \beta_2 I^H \frac{S}{M} - \gamma I^H - \min(\lambda I^H, \lambda I^H_{\max}) + \Phi_t. \tag{31}$$

We observe that the metastable regime's key ingredients relate to TTI: The system reacts less intensively to new infections when case numbers are below the TTI capacity, as infection chains are diligently found and removed. On the other hand, when the TTI system is overwhelmed, infections reproduce at the natural, hidden rate. Assuming quasi-stationary dynamics for the susceptible pool (S), we can approximate:

$$\frac{d}{dI^H}\left(\frac{dI^H}{dt}\right) = \begin{cases} \beta_2 \dfrac{S}{M} - \gamma - \lambda, & \text{if } I^H < I^H_{\max}, \\ \\ \beta_2 \dfrac{S}{M} - \gamma, & \text{otherwise.} \end{cases} \tag{32}$$

If I^H exceeds $I^H_{\max}$, there is the possibility for I^H to grow and lead to a more significant number of cases for a broader range of parameters. On the other hand, when studying the linear system's equilibrium,

we identify the contributions to the observed number of cases $\hat{N}_\infty^{\text{obs}} = \beta_1 I_\infty^Q + \lambda I_\infty^H$. Assuming stationary conditions for the $\frac{S}{M} \approx 1$ limit, we obtain:

$$\hat{N}_\infty^{\text{obs}} = \frac{\Phi_t}{\lambda + \gamma - \beta_2} \frac{\gamma\lambda}{\gamma - \beta_1}. \tag{33}$$

Using these simple models, we can better understand the parameters and mechanisms that render the system unstable or the equilibrium unfeasible. This better understanding of factors contributing to stabilizing –and respectively destabilizing– the system, helps to guide policies. The transitions and equilibrium levels have more complex analytical expressions in our model but follow the same spirit: to draw the line between the stable and unstable spread.

S1.8 Exploring the effect of more compartments for the exposed individuals

Compartmental models coupled with differential equations implicitly assume first-order kinetics, which translates to exponential emptying or filling the compartments involved in the dynamics. Even though the expected residence time can be set for each compartment, the exponential shape of the residence time distribution differs from the true disease dynamics. This difference can be corrected by including extra compartments, so instead of having an exponential shape, the residence time distribution eventually converges to a delta distribution around the desired value. Aiming to evaluate how this effect might change our estimates for k_t^{crit}, we included three compartments for the exposed fraction of the population (and for hidden and quarantined infections) presented in Fig. S6. As the latent period would be spent in these compartments, the residence time in each one is one-third of the original, so that the new transition rate would be $\rho' = 3\rho$.

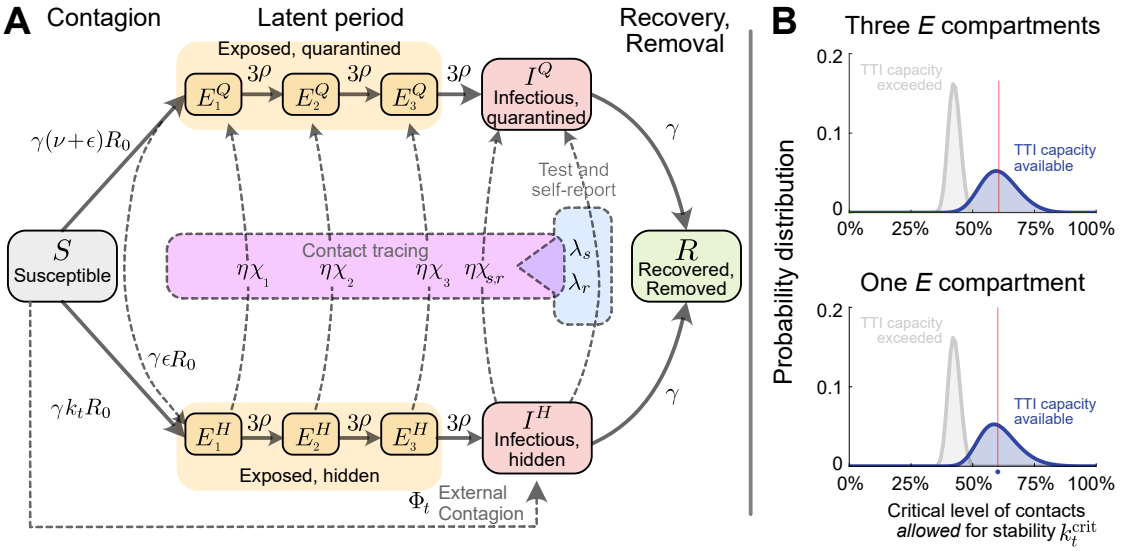

Supplementary Figure S6: **Flowchart of the complete model, including three compartments for the latent period. A:** The solid blocks in the diagram represent different SEIR compartments for both hidden and quarantined individuals. Hidden cases are further divided into symptomatic and asymptomatic carriers (not shown). Solid lines represent the natural progression of the infection (contagion, latent period, and recovery). On the other hand, dashed lines account for imperfect quarantine and limited compliance, external factors, and test-trace-and-isolate policies. **B:** Comparison between the distribution of k_t^{crit} for the single-compartment model and the three compartments model.

Following the same formalism presented in the previous sections, we estimate the fraction of individuals infected at time t that would remain in the different compartments by the time of contact tracing.

$$\chi_1 = \exp\left(-3\rho\tau\right), \tag{34}$$

$$\chi_2 = (3\rho)\,\tau \exp\left(-3\rho\tau\right), \tag{35}$$

$$\chi_3 = (3\rho)^2 \frac{\tau^2}{2} \exp\left(-3\rho\tau\right). \tag{36}$$

Consistently, we can demonstrate that the fraction of individuals staying in the infectious compartment in the presence of symptom-based testing is given by

$$\chi_{s,r} = \begin{cases} (3\rho)^3 \dfrac{\tau^3}{3!} \exp\left(-3\rho\tau\right), & \text{if } 3\rho \approx \lambda_s + \lambda_r \\ \dfrac{(3\rho)^3 \exp\left(-3\rho\tau\right)}{2(\lambda_s+\lambda_r-3\rho)} \left(\tau^2 - 2\dfrac{\tau}{\lambda_s+\lambda_r-3\rho} + \dfrac{2}{(\lambda_s+\lambda_r-3\rho)^2}\left(1-\exp\left(-\tau\left(\lambda_s+\lambda_r-3\rho\right)\right)\right)\right), & \text{else.} \end{cases} \tag{37}$$

To analyze the stability of the extended system with three exposed compartments, we proceeded as described in Section S1.2. The linear system with delay representing the dynamics is $x'(t) = Ax(t) + Bx(t-\tau)$, with $x(t) = \left[E_1^Q(t);\, E_2^Q(t);\, E_3^Q(t);\, E_1^H(t);\, E_2^H(t);\, E_3^H(t);\, I^Q(t);\, I^H(t);\, I^{H,s}(t)\right]$, where matrices A and B are given by:

$$A = \begin{pmatrix} -3\rho & 0 & 0 & 0 & 0 & 0 & \nu\gamma R_0 & 0 & 0 \\ 3\rho & -3\rho & 0 & 0 & 0 & 0 & 0 & 0 & 0 \\ 0 & 3\rho & -3\rho & 0 & 0 & 0 & 0 & 0 & 0 \\ 0 & 0 & 0 & -3\rho & 0 & 0 & \epsilon\gamma R_0 & \gamma k_t R_0 & 0 \\ 0 & 0 & 0 & 3\rho & -3\rho & 0 & 0 & 0 & 0 \\ 0 & 0 & 0 & 0 & 3\rho & -3\rho & 0 & 0 & 0 \\ 0 & 0 & 3\rho & 0 & 0 & 0 & -\gamma & \lambda_r & \lambda_s \\ 0 & 0 & 0 & 0 & 0 & 3\rho & 0 & -\gamma-\lambda_r & -\lambda_s \\ 0 & 0 & 0 & 0 & 0 & 3\left(1-\xi\right)\rho & 0 & 0 & -\gamma-\lambda_r-\lambda_s \end{pmatrix} \tag{38}$$

$$B = \begin{pmatrix} 0 & 0 & 0 & 0 & 0 & 0 & \lambda_r^{\text{eff}}\chi_1 & \lambda_s^{\text{eff}}\chi_1 \\ 0 & 0 & 0 & 0 & 0 & 0 & \lambda_r^{\text{eff}}\chi_2 & \lambda_s^{\text{eff}}\chi_2 \\ 0 & 0 & 0 & 0 & 0 & 0 & \lambda_r^{\text{eff}}\chi_3 & \lambda_s^{\text{eff}}\chi_3 \\ 0 & 0 & 0 & 0 & 0 & 0 & -\lambda_r^{\text{eff}}\chi_1 & -\lambda_s^{\text{eff}}\chi_1 \\ 0 & 0 & 0 & 0 & 0 & 0 & -\lambda_r^{\text{eff}}\chi_2 & -\lambda_s^{\text{eff}}\chi_2 \\ 0 & 0 & 0 & 0 & 0 & 0 & -\lambda_r^{\text{eff}}\chi_3 & -\lambda_s^{\text{eff}}\chi_3 \\ 0 & 0 & 0 & 0 & 0 & 0 & \lambda_r^{\text{eff}}\left(\xi\chi_r + \left(1-\xi\right)\chi_{s,r}\right) & \lambda_s^{\text{eff}}\left(\xi\chi_r + \left(1-\xi\right)\chi_{s,r}\right) \\ 0 & 0 & 0 & 0 & 0 & 0 & -\lambda_r^{\text{eff}}\left(\xi\chi_r + \left(1-\xi\right)\chi_{s,r}\right) & -\lambda_s^{\text{eff}}\left(\xi\chi_r + \left(1-\xi\right)\chi_{s,r}\right) \\ 0 & 0 & 0 & 0 & 0 & 0 & -\lambda_r^{\text{eff}}\left(1-\xi\right)\chi_{s,r} & -\lambda_s^{\text{eff}}\left(1-\xi\right)\chi_{s,r} \end{pmatrix} \eta k_t R_0, \tag{39}$$

We obtained new estimates for k_t^{crit} in the cases of available TTI capacity and overwhelmed TTI capacity. Comparing these values to those obtained in our original model (with a single exposed compartment), we find that they do not deviate significantly. Graphically, we see that the distributions share the same properties, being slightly less skewed in the three-compartment case (see Fig. S6B). In numbers, the relative error we induce in calculating the critical level of contacts allowed for stability by using a single exposed compartment instead of three is reported in table S3.

Supplementary Table S3: Linearly-derived correspondence between contact reduction and the observed reproduction number (7.5e4 realizations).

		Percentile		
Variable		2.5 %	50 % (median)	97.5 %
$k_t^{\text{crit}}\big\vert_{\text{no TTI}}$	three compartments	37.80 %	42.58 %	46.68 %
	one compartment	37.71 %	42.59 %	46.71 %
$k_t^{\text{crit}}\big\vert_{\text{TTI}}$	three compartments	47.19 %	60.60 %	76.39 %
	one compartment	46.99 %	60.48 %	76.20 %
Relative error	no TTI	0.22 %	0.03 %	0.07 %
	TTI	0.42 %	0.19 %	0.24 %

REFERENCES AND NOTES

1. H. E. Randolph, L. B. Barreiro, Herd immunity: Understanding COVID-19. *Immunity* **52**, 737–741 (2020).
2. A. T. Levin, W. P. Hanage, N. Owusu-Boaitey, K. B. Cochran, S. P. Walsh, G. Meyerowitz-Katz, Assessing the age specificity of infection fatality rates for COVID-19: Systematic review, meta-analysis, and public policy implications. *Eur. J. Epidemiol.* **35**, 1123–1138 (2020).
3. N. A. Alwan, R. A. Burgess, S. Ashworth, R. Beale, N. Bhadelia, D. Bogaert, J. Dowd, I. Eckerle, L. R. Goldman, T. Greenhalgh, D. Gurdasani, A. Hamdy, W. P. Hanage, E. B. Hodcroft, Z. Hyde, P. Kellam, M. Kelly-Irving, F. Krammer, M. Lipsitch, A. McNally, M. McKee, A. Nouri, D. Pimenta, V. Priesemann, H. Rutter, J. Silver, D. Sridhar, C. Swanton, R. P. Walensky, G. Yamey, H. Ziauddeen, Scientific consensus on the COVID-19 pandemic: We need to act now. *Lancet* **396**, e71–e72 (2020).
4. E. Fraser, Long term respiratory complications of COVID-19. *BMJ* **370**, m3001 (2020).
5. T. Greenhalgh, M. Knight, C. A Ćourt, M. Buxton, L. Husain, Management of post-acute COVID-19 in primary care. *BMJ* **370**, m3026 (2020).
6. E. J. Topol, COVID-19 can affect the heart. *Science* **370**, 408–409 (2020).
7. V. Priesemann, M. M. Brinkmann, S. Ciesek, S. Cuschieri, T. Czypionka, G. Giordano, D. Gurdasani, C. Hanson, N. Hens, E. Iftekhar, M. Kelly-Irving, P. Klimek, M. Kretzschmar, A. Peichl, M. Perc, F. Sannino, E. Schernhammer, A. Schmidt, A. Staines, E. Szczurek, Calling for pan-European commitment for rapid and sustained reduction in SARS-CoV-2 infections. *Lancet* **397**, 92–93 (2021).
8. A. Scherbina, Determining the optimal duration of the COVID-19 suppression policy: A cost-benefit analysis (2019); https://ssrn.com/abstract=3562053.
9. J. Xiong, O. Lipsitz, F. Nasri, L. M. Lui, H. Gill, L. Phan, D. Chen-Li, M. Iacobucci, R. Ho, A. Majeed, R. S. McIntyre, Impact of COVID-19 pandemic on mental health in the general population: A systematic review. *J. Affect. Disord.* **277**, 55–64 (2020).
10. R. Li, S. Pei, B. Chen, Y. Song, T. Zhang, W. Yang, J. Shaman, Substantial undocumented infection facilitates the rapid dissemination of novel coronavirus (SARS-CoV-2). *Science* **368**, 489–493 (2020).
11. N. Van Doremalen, T. Bushmaker, D. H. Morris, M. G. Holbrook, A. Gamble, B. N. Williamson, A. Tamin, J. L. Harcourt, N. J. Thornburg, S. I. Gerber, J. O. Lloyd-Smith, E. de Wit, V. J. Munster,

Aerosol and surface stability of SARS-CoV-2 as compared with SARS-CoV-1. *N. Engl. J. Med.* **382**, 1564–1567 (2020).

12. S. Moore, E. M. Hill, M. J. Tildesley, L. Dyson, M. J. Keeling, Vaccination and non-pharmaceutical interventions for COVID-19: A mathematical modelling study. *Lancet Infect. Dis.* **21**, 793–802 (2021).
13. S. Bauer, S. Contreras, J. Dehning, M. Linden, E. Iftekhar, S. B. Mohr, Á. Olivera-Nappa, V. Priesemann, Relaxing restrictions at the pace of vaccination increases freedom and guards against further COVID-19 waves in Europe. arXiv:2103.06228 [q-bio.PE] (2021).
14. S. Contreras, V. Priesemann, Risking further COVID-19 waves despite vaccination. *Lancet Infect. Dis.* **21**, 745–746 (2021).
15. S. Contreras, J. Dehning, M. Loidolt, J. Zierenberg, F. P. Spitzner, J. H. Urrea-Quintero, S. B. Mohr, M. Wilczek, M. Wibral, V. Priesemann, The challenges of containing SARS-CoV-2 via test-trace-and-isolate. *Nat. Commun.* **12**, 378 (2021).
16. M. Linden, S. B. Mohr, J. Dehning, J. Mohring, M. Meyer-Hermann, I. Pigeot, A. Schöbel, V. Priesemann, Case numbers beyond contact tracing capacity are endangering the containment of COVID-19. *Dtsch. Arztebl. Int.* **117**, 790–791 (2020).
17. J. Dehning, J. Zierenberg, F. P. Spitzner, M. Wibral, J. P. Neto, M. Wilczek, V. Priesemann, Inferring change points in the spread of COVID-19 reveals the effectiveness of interventions. *Science* **369**, eabb9789 (2020).
18. H. W. Hethcote, The mathematics of infectious diseases. *SIAM Rev.* **42**, 599–653 (2000).
19. S. Zhao, Q. Lin, J. Ran, S. S. Musa, G. Yang, W. Wang, Y. Lou, D. Gao, L. Yang, D. He, M. H. Wang, Preliminary estimation of the basic reproduction number of novel coronavirus (2019-nCoV) in china, from 2019 to 2020: A data-driven analysis in the early phase of the outbreak. *Int. J. Infect. Dis.* **92**, 214–217 (2020).
20. Y. Alimohamadi, M. Taghdir, M. Sepandi, Estimate of the basic reproduction number for COVID-19: A systematic review and meta-analysis. *J. Prev. Med. Public Health* **53**, 151–157 (2020).
21. J. P. La Salle, *The Stability of Dynamical Systems* (SIAM, 1976).
22. J. Wilting, V. Priesemann, Inferring collective dynamical states from widely unobserved systems. *Nat. Commun.* **9**, 2325 (2018).

23. M. J. Keeling, G. Guyver-Fletcher, A. Holmes, L. Dyson, M. J. Tildesley, E. M. Hill, G. F. Medley, Precautionary breaks: Planned, limited duration circuit breaks to control the prevalence of COVID-19. *medRxiv* 2020.10.13.20211813 (2020).
24. E. Mahase, COVID-19: Experts recommend two week circuit break to reduce transmission in the UK. *BMJ* **371**, m4038 (2020).
25. Z. Kmietowicz, Covid-19: "There is no alternative," says Johnson, announcing new restrictions for England. *BMJ* **371**, m4247 (2020).
26. J. M. Brauner, S. Mindermann, M. Sharma, D. Johnston, J. Salvatier, T. Gavenčiak, A. B. Stephenson, G. Leech, G. Altman, V. Mikulik, A. J. Norman, J. T. Monrad, T. Besiroglu, H. Ge, M. A. Hartwick, Y. W. Teh, L. Chindelevitch, Y. Gal, J. Kulveit, Inferring the effectiveness of government interventions against covid-19. *Science* **371**, eabd9338 (2021).
27. Y. Li, H. Campbell, D. Kulkarni, A. Harpur, M. Nundy, X. Wang, H. Nair, The temporal association of introducing and lifting non-pharmaceutical interventions with the time-varying reproduction number (R) of SARS-CoV-2: A modelling study across 131 countries. *Lancet Infect. Dis.* **21**, 193–202 (2020).
28. E. Holt, Slovakia to test all adults for SARS-CoV-2. *Lancet* **396**, 1386–1387 (2020).
29. M. J. Mina, R. Parker, D. B. Larremore, Rethinking Covid-19 test sensitivity—A strategy for containment. *N. Engl. J. Med.* **383**, e120 (2020).
30. D. B. Larremore, B. Wilder, E. Lester, S. Shehata, J. M. Burke, J. A. Hay, M. Tambe, M. J. Mina, R. Parker, Test sensitivity is secondary to frequency and turnaround time for COVID-19 screening. *Sci. Adv.* **7**, eabd5393 (2021).
31. R. D. Kirkcaldy, B. A. King, J. T. Brooks, COVID-19 and postinfection immunity: Limited evidence, many remaining questions, *JAMA* **323**, 2245–2246 (2020).
32. M. Thompson, J. Burgess, A. Naleway, H. L. Tyner, S. K. Yoon, J. Meece, L. E. W. Olsho, A. J. Caban-Martinez, A. Fowlkes, K. Lutrick, J. L. Kuntz, K. Dunnigan, M. J. Odean, K. T. Hegmann, E. Stefanski, L. J. Edwards, N. Schaefer-Solle, L. Grant, K. Ellingson, H. C. Groom, T. Zunie, M. S. Thiese, L. Ivacic, M. G. Wesley, J. M. Lamberte, X. Sun, M. E. Smith, A. L. Phillips, K. D. Groover, Y. M. Yoo, J. Gerald, R. T. Brown, M. K. Herring, G. Joseph, S. Beitel, T. C. Morrill, J. Mak, P. Rivers, K. M. Harris, D. R. Hunt, M. L. Arvay, P. Kutty, A. M. Fry, M. Gaglani, Interim estimates of vaccine effectiveness of BNT162b2 and mRNA-1273 COVID-19 vaccines in preventing SARS-CoV-2 infection among health care personnel, first responders, and other essential

and frontline workers—Eight U.S. locations, December 2020–March 2021. *MMWR Morb. Mortal. Wkly. Rep.* **70**, 495–500 (2021).

33. N. Dagan, N. Barda, E. Kepten, O. Miron, S. Perchik, M. A. Katz, M. A. Hernán, M. Lipsitch, B. Reis, R. D. Balicer, BNT162b2 mRNA Covid-19 vaccine in a nationwide mass vaccination setting. *N. Engl. J. Med.* **384**, 1412–1423 (2021).
34. M. Voysey, S. A. C. Clemens, S. A. Madhi, L. Y. Weckx, P. M. Folegatti, P. K. Aley, B. Angus, V. L. Baillie, S. L. Barnabas, Q. E. Bhorat, S. Bibi, C. Briner, P. Cicconi, A. M. Collins, R. Colin-Jones, C. L. Cutland, T. C. Darton, K. Dheda, C. J. A. Duncan, K. R. W. Emary, K. J. Ewer, L. Fairlie, S. N. Faust, S. Feng, D. M. Ferreira, A. Finn, A. L. Goodman, C. M. Green, C. A. Green, P. T. Heath, C. Hill, H. Hill, I. Hirsch, S. H. C. Hodgson, A. Izu, S. Jackson, D. Jenkin, C. C. D. Joe, S. Kerridge, A. Koen, G. Kwatra, R. Lazarus, A. M. Lawrie, A. Lelliott, V. Libri, P. J. Lillie, R. Mallory, A. V. A. Mendes, E. P. Milan, A. M. Minassian, A. M. Gregor, H. Morrison, Y. F. Mujadidi, A. Nana, P. J O'Reilly, S. D. Padayachee, A. Pittella, E. Plested, K. M. Pollock, M. N. Ramasamy, S. Rhead, A. V. Schwarzbold, N. Singh, A. Smith, R. Song, M. D. Snape, E. Sprinz, R. K. Sutherland, R. Tarrant, E. C. Thomson, M. Estée Török, M. Toshner, D. P. J. Turner, J. Vekemans, T. L. Villafana, M. E. E. Watson, C. J. Williams, A. D. Douglas, A. V. S. Hill, T. Lambe, S. C. Gilbert, A. J. Pollard; Oxford COVID Vaccine Trial Group, Safety and efficacy of the ChAdOx1 nCoV-19 vaccine (AZD1222) against SARS-CoV-2: An interim analysis of four randomised controlled trials in Brazil, South Africa, and the UK. *Lancet* **397**, 99–111 (2021).
35. T. Hale, S. Webster, A. Petherick, T. Phillips, B. Kira, Oxford COVID-19 Government Response Tracker, Blavatnik School of Government (2020); www.fda.gov/media/136472/download.
36. A. J. Kucharski, P. Klepac, A. J. K. Conlan, S. M. Kissler, M. L. Tang, H. Fry, J. R. Gog, W. J. Edmunds; CMMID COVID-19 working group, Effectiveness of isolation, testing, contact tracing, and physical distancing on reducing transmission of SARS-CoV-2 in different settings: A mathematical modelling study. *Lancet Infect. Dis.* **20**, 1151–1160 (2020).
37. C. C. Kerr, D. Mistry, R. M. Stuart, K. Rosenfeld, G. R. Hart, R. C. Núñez, J. A. Cohen, P. Selvaraj, R. G. Abeysuriya, M. Jastrzebski, L. George, B. Hagedorn, J. Panovska-Griffiths, M. Fagalde, J. Duchin, M. Famulare, D. J. Klein, Controlling COVID-19 via test-trace-quarantine. *Nat. Commun.* **12**, 2993 (2021).
38. C. Fraser, S. Riley, R. M. Anderson, N. M. Ferguson, Factors that make an infectious disease outbreak controllable. *Proc. Natl. Acad. Sci. U.S.A.* **101**, 6146–6151 (2004).

39. L. Ferretti, C. Wymant, M. Kendall, L. Zhao, A. Nurtay, L. Abeler-Dörner, M. Parker, D. Bonsall, C. Fraser, Quantifying SARS-CoV-2 transmission suggests epidemic control with digital contact tracing. *Science* **368**, eabb6936 (2020).
40. D. Lunz, G. Batt, J. Ruess, To quarantine, or not to quarantine: A theoretical framework for disease control via contact tracing. *Epidemics* **34**, 100428 (2021).
41. S. Sturniolo, W. Waites, T. Colbourn, D. Manheim, J. Panovska-Griffiths, Testing, tracing and isolation in compartmental models. *PLOS Comput. Biol.* **17**, e1008633 (2021).
42. J. Hellewell, S. Abbott, A. Gimma, N. I. Bosse, C. I. Jarvis, T. W. Russell, J. D. Munday, A. J. Kucharski, W. J. Edmunds, F. Sun, Feasibility of controlling COVID-19 outbreaks by isolation of cases and contacts. *Lancet Glob. Health* **8**, e488–e496 (2020).
43. E. L. Davis, T. C. D. Lucas, A. Borlase, T. M. Pollington, S. Abbott, D. Ayabina, T. Crellen, J. Hellewell, L. Pi; CMMID COVID-19 working group, G. F. Medley, T. Déirdre Hollingsworth, P. Klepac, An imperfect tool: COVID-19'test & trace' success relies on minimising the impact of false negatives and continuation of physical distancing. *medRxiv*, 2020.06.09.20124008 (2020).
44. J. J. Van Bavel, K. Baicker, P. S. Boggio, V. Capraro, A. Cichocka, M. Cikara, M. J. Crockett, A. J. Crum, K. M. Douglas, J. N. Druckman, J. Drury, O. Dube, N. Ellemers, E. J. Finkel, J. H. Fowler, M. Gelfand, S. Han, S. A. Haslam, J. Jetten, S. Kitayama, D. Mobbs, L. E. Napper, D. J. Packer, G. Pennycook, E. Peters, R. E. Petty, D. G. Rand, S. D. Reicher, S. Schnall, A. Shariff, L. J. Skitka, S. S. Smith, C. R. Sunstein, N. Tabri, J. A. Tucker, S. van der Linden, P. van Lange, K. A. Weeden, M. J. A. Wohl, J. Zaki, S. R. Zion, R. Willer, Using social and behavioural science to support COVID-19 pandemic response. *Nat. Hum. Behav.* **4**, 460–471 (2020).
45. S. Hsiang, D. Allen, S. Annan-Phan, K. Bell, I. Bolliger, T. Chong, H. Druckenmiller, L. Y. Huang, A. Hultgren, E. Krasovich, P. Lau, J. Lee, E. Rolf, J. Tseng, T. Wu, The effect of large-scale anti-contagion policies on the COVID-19 pandemic. *Nature* **584**, 262–267 (2020).
46. M. Sharma, S. Mindermann, C. Rogers-Smith, G. Leech, B. Snodin, J. Ahuja, J. B. Sandbrink, J. T. Monrad, G. Altman, G. Dhaliwal, L. Finnveden, A. J. Norman, S. B. Oehm, J. F. Sandkühler, T. Mellan, J. Kulveit, L. Chindelevitch, S. Flaxman, Y. Gal, S. Mishra, J. M. Brauner, S. Bhatt, Understanding the effectiveness of government interventions in Europe's second wave of COVID-19. *medRxiv* 2021.03.25.21254330 (2021).
47. D. K. Chu, E. A. Akl, S. Duda, K. Solo, S. Yaacoub, H. J. Schünemann; COVID-19 Systematic Urgent Review Group Effort (SURGE) study authors, Physical distancing, face masks, and eye

protection to prevent person-to-person transmission of SARS-CoV-2 and COVID-19: A systematic review and meta-analysis. *Lancet* **395**, 1973–1987 (2020).

48. J. Howard, A. Huang, Z. Li, Z. Tufekci, V. Zdimal, H.-M. van der Westhuizen, A. von Delft, A. Price, L. Fridman, L.-H. Tang, V. Tang, G. L. Watson, C. E. Bax, R. Shaikh, F. Questier, D. Hernandez, L. F. Chu, C. M. Ramirez, A. W. Rimoin, An evidence review of face masks against COVID-19. *Proc. Natl. Acad. Sci. U.S.A* **118**, e2014564118 (2021).
49. J. H. McDermott, W. G. Newman, Refusal of viral testing during the SARS-CoV-2 pandemic. *Clin. Med.* **20**, e163, e164 (2020).
50. C.-C. Lai, Y. H. Liu, C.-Y. Wang, Y.-H. Wang, S.-C. Hsueh, M.-Y. Yen, W.-C. Ko, P.-R. Hsueh, Asymptomatic carrier state, acute respiratory disease, and pneumonia due to severe acute respiratory syndrome coronavirus 2 (SARS-CoV-2): Facts and myths. *J. Microbiol. Immunol. Infect.* **53**, 404-412 (2020).
51. E. Lavezzo, E. Franchin, C. Ciavarella, G. Cuomo-Dannenburg, L. Barzon, C. Del Vecchio, L. Rossi, R. Manganelli, A. Loregian, N. Navarin, D. Abate, M. Sciro, S. Merigliano, E. De Canale, M. C. Vanuzzo, V. Besutti, F. Saluzzo, F. Onelia, M. Pacenti, S. G. Parisi, G. Carretta, D. Donato, L. Flor, S. Cocchio, G. Masi, A. Sperduti, L. Cattarino, R. Salvador, M. Nicoletti, F. Caldart, G. Castelli, E. Nieddu, B. Labella, L. Fava, M. Drigo, K. A. M. Gaythorpe; Imperial College COVID-Response Team, A. R. Brazzale, S. Toppo, M. Trevisan, V. Baldo, C. A. Donnelly, N. M. Ferguson, I. Dorigatti, A. Crisanti, Suppression of COVID-19 outbreak in the municipality of Vo, Italy. *Nature* **584**, 425-429 (2020).
52. O. Byambasuren, M. Cardona, K. Bell, J. Clark, M.-L. McLaws, P. Glasziou, Estimating the extent of asymptomatic COVID-19 and its potential for community transmission: Systematic review and meta-analysis. *J. Assoc. Med. Microbiol. Infect. Dis. Canada* **5**, 223–234 (2020).
53. M. Cevik, K. Kuppalli, J. Kindrachuk, M. Peiris, Virology, transmission, and pathogenesis of SARS-CoV-2. *BMJ* **371**, m3862 (2020).
54. M. Pollán, B. Pérez-Gómez, R. Pastor-Barriuso, J. Oteo, M. A. Hernán, M. Pérez-Olmeda, J. L. Sanmartín, A. Fernández-García, I. Cruz, N. F. de Larrea, M. Molina, F. Rodríguez-Cabrera, M. Martín, P. Merino-Amador, J. L. Paniagua, J. F. Muñoz-Montalvo, F. Blanco, R. Yotti; ENE-COVID Study Group, Prevalence of sars-cov-2 in spain (ene-covid): A nationwide, population-based seroepidemiological study. *Lancet* **396**, 535–544 (2020).

55. J. A. Firth, J. Hellewell, P. Klepac, S. M. Kissler, A. J. Kucharski, L. G. Spurgin, Combining fine-scale social contact data with epidemic modelling reveals interactions between contact tracing, quarantine, testing and physical distancing for controlling COVID-19. *medRxiv* 10.1101/2020.05.26.20113720 (2020).
56. S. Kojaku, L. Hébert-Dufresne, E. Mones, S. Lehmann, Y.-Y. Ahn, The effectiveness of backward contact tracing in networks. *Nat. Phys.* **17**, 652–658 (2021).
57. F. P. Polack, S. J. Thomas, N. Kitchin, J. Absalon, A. Gurtman, S. Lockhart, J. L. Perez, G. Pérez Marc, E. D. Moreira, C. Zerbini, R. Bailey, K. A. Swanson, S. Roychoudhury, K. Koury, P. Li, W. V. Kalina, D. Cooper, R. W. Frenck Jr., L. L. Hammitt, Ö. Türeci, H. Nell, A. Schaefer, S. Ünal, D. B. Tresnan, S. Mather, P. R. Dormitzer, U. Şahin, K. U. Jansen, W. C. Gruber, C4591001 Clinical Trial Group., Safety and efficacy of the bnt162b2 mrna covid-19 vaccine. *N. Engl. J. Med.* **383**, 2603–2615 (2020).
58. M. an der Heiden, O. Hamouda, Schätzung der aktuellen Entwicklung der SARS-CoV-2- Epidemie in Deutschland – Nowcasting. *Epidemiologisches Bull.* **2020**, 10–15 (2020).
59. L. F. Shampine, S. Thompson, Solving ddes in matlab. *Appl. Numer. Math.* **37**, 441–458 (2001).
60. E. Jarlebring, Some numerical methods to compute the eigenvalues of a time-delay system using MATLAB. *E-Delay System Letter* **2**, 155 (2008).
61. L. N. Trefethen, *Spectral Methods in MATLAB* (SIAM, 2000).
62. H. Ritchie, E. Mathieu, L. Rodés-Guirao, C. Appel, C. Giattino, E. Ortiz-Ospina, J. Hasell, B. Macdonald, D. Beltekian, M. Roser, Coronavirus pandemic (COVID-19), *Our World in Data* (2020); https://ourworldindata.org/coronavirus.
63. J. Dehning, Priesemann-Group/covid19_metastability. Zenodo (2021); https://doi.org/10.5281/zenodo.5220793.
64. X. He, E. H. Y. Lau, P. Wu, X. Deng, J. Wang, X. Hao, Y. C. Lau, J. Y. Wong, Y. Guan, X. Tan, X. Mo, Y. Chen, B. Liao, W. Chen, F. Hu, Q. Zhang, M. Zhong, Y. Wu, L. Zhao, F. Zhang, B. J. Cowling, F. Li, G. M. Leung, Temporal dynamics in viral shedding and transmissibility of COVID-19. *Nat. Med.* 1491–1493 (2020).
65. F. Pan, T. Ye, P. Sun, S. Gui, B. Liang, L. Li, D. Zheng, J. Wang, R. L. Hesketh, L. Yang, C. Zheng, Time course of lung changes on chest CT during recovery from 2019 novel coronavirus (COVID-19) pneumonia. *Radiology* **295**, 200370 (2020).

66. Y. M. Bar-On, A. Flamholz, R. Phillips, R. Milo, SARS-CoV-2 (COVID-19) by the numbers. *eLife* **9**, e57309 (2020).
67. A. F. Siegenfeld, Y. Bar-Yam, The impact of travel and timing in eliminating COVID-19. *Commun. Phys.* **3**, 204 (2020).
68. P. Bittihn, R. Golestanian, Containment strategy for an epidemic based on fluctuations in the SIR model. arXiv:2003.08784 [q-bio.PE] (2020).
69. J. Salvatier, T. V. Wiecki, C. Fonnesbeck, Probabilistic programming in Python using PyMC3. *PeerJ Comput. Sci.* **2**, e55 (2016).